Inorganic Chemistry

Article

pubs.acs.org/IC

What Determines Catalyst Functionality in Molecular Water Oxidation? Dependence on Ligands and Metal Nuclearity in Cobalt Clusters

Paul F. Smith,[†] Christopher Kaplan,[†] John E. Sheats, David M. Robinson, Nicholas S. McCool, Nicholas Mezle, and G. Charles Dismukes*

Department of Chemistry and Chemical Biology, Rutgers University, 610 Taylor Road, Piscataway, New Jersy 08854, United States

Supporting Information

ABSTRACT: The metal-oxo M_4O_4 "cubane" topology is of special significance to the field of water oxidation as it represents the merging of bioinspired structural principles derived from natural photosynthesis with successful artificial catalysts known to date. Herein, we directly compare the rates of water oxidation/O_2 evolution catalyzed by six cobalt−oxo clusters including the Co_4O_4 cubanes, $Co_4O_4(OAc)_4(py)_4$ and $[Co_4O_4(OAc)_2(bpy)_4]^{2+}$, using the common $Ru(bpy)_3^{2+}$/$S_2O_8^{2-}$ photo-oxidant assay. At pH 8, the first-order rate constants for these cubanes differ by 2-fold, 0.030 and 0.015 s^{-1}, respectively, reflecting the number of labile carboxylate sites that allow substrate water binding in a pre-equilibrium step before O_2 release. Kinetic results reveal a deprotonation step occurs on this pathway and that two electrons are removed before O_2 evolution occurs. The Co_4O_4 cubane core is shown to be the smallest catalytic unit for the intramolecular water oxidation pathway, as neither "incomplete cubane" trimers $[Co_3O(OH)_3(OAc)_2(bpy)_3]^{2+}$ and $[Co_3O(OH)_2(OAc)_3(py)_5]^{2+}$ nor "half cubane" dimers $[Co_2(OH)_2(OAc)_3(bpy)_2]^{+}$ and $[Co_2(OH)_2(OAc)_3(py)_4]^{+}$ were found capable of evolving O_2, despite having the same ligand sets as their cubane counterparts. Electrochemical studies reveal that oxidation of both cubanes to formally Co_4(3III,IV) (0.7 V vs Ag/AgCl) occurs readily, while neither dimers nor trimers are oxidized below 1.5 V, pointing to appreciably greater charge delocalization in the $[Co_4O_4]^{5+}$ core. The origin of catalytic activity by Co_4O_4 cubanes illustrates three key features for water oxidation: (1) four one-electron redox metals, (2) efficient charge delocalization of the first oxidation step across the Co_4O_4 cluster, allowing for stabilization of higher oxidizing equivalents, and (3) terminal coordination site for substrate aquo/oxo formation.

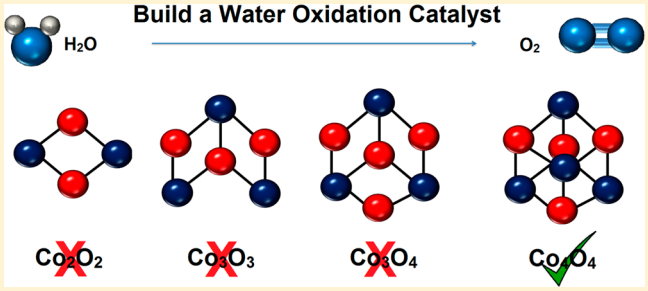

INTRODUCTION

Water oxidation catalysts based on first row transition ions are widely sought as replacements for costly noble metal catalysts. Numerous examples of molecular catalysts have been studied which operate over a wide range of cluster nuclearities, ligand functionalities, kinetic activities, and energy efficiencies.[1−10] Systematic studies within families of related catalysts have uncovered mechanistic complexities that have hampered understanding the factors that influence the rate of O_2 production and the catalyst lifetime.

As a reference point, oxygenic photosynthesis is capable of photo-oxidizing water far faster than any artificial catalyst based on first row transition metals. A recent analysis of the 1.9 Å resolved crystal structure of Photosystem II has shown that nature's universally conserved water oxidation catalyst is a $CaMn_4O_5$ cluster best described as a $CaMn_3O_4$ "heterocubane" with an O−Mn "dangler".[11] As result, molecular tetrametallic clusters are increasingly reported as water oxidation catalysts.[12] Among these, the Co_4O_4 cubane structure has been found highly active among metal−oxide molecular catalysts.[13−15] It also serves as a simplified model for several heterogeneous metal oxide catalysts that contain cubical Co_4O_4 and Mn_4O_4 subunits, respectively,[16] notably the spinels Co_3O_4[17] and λ-MnO_2,[18] cubic $LiCoO_2$,[19] and studies which conjecture that cubic structures may form in the amorphous Co-Pi catalyst.[20−22]

A particularly clear example of the benefit of the cubical topology for catalysis is seen among the two polymorphs of $LiCoO_2$ which differ by 100-fold in catalytic activity. Layered $LiCoO_2$ is made up of alternating layers of cobalt oxide composed of "incomplete cubane" Co_3O_4 replicas, and lithium oxide layers. This material is catalytically inactive.[19] By contrast, active cubic $LiCoO_2$ is composed of Co_4O_4 cubes stitched together by lithium ions at the corner oxos. This research inspired us to analyze clusters resembling fractions of the Co_4O_4 cubane to determine the required Co nuclearity and other properties needed for catalysis.

In this work we examine the influence of cluster nuclearity and ligand type on the kinetics of water oxidation among the six

Received: October 29, 2013
Published: February 5, 2014

   dx.doi.org/10.1021/ic402720p | Inorg. Chem. 2014, 53, 2113−2121

cobalt clusters depicted in Scheme 1. These compounds represent the gradual building of the M_4O_4 cubical core of

Scheme 1. Compounds and Photoassay Used in This Article

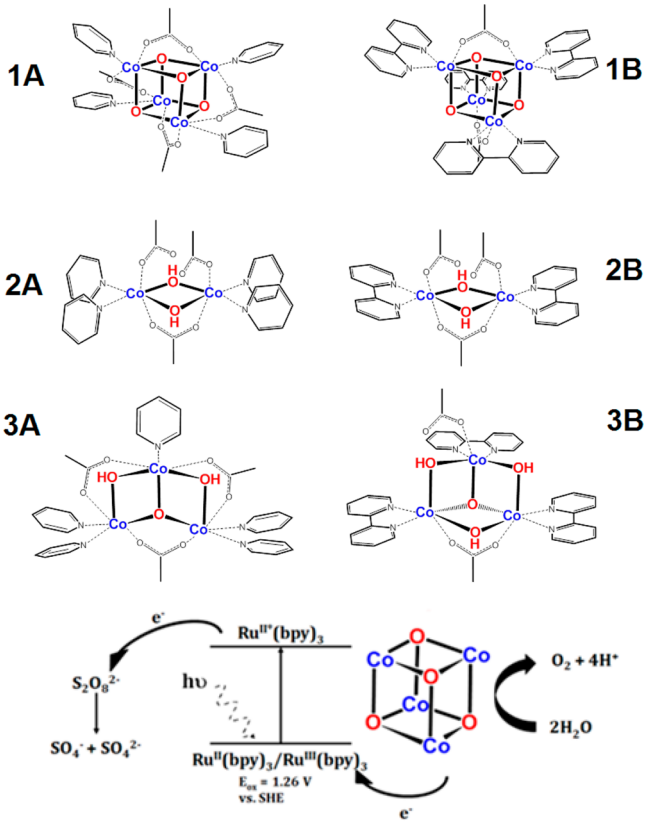

interest *within the same ligand sets* (acetate and either pyridine or bipyridine). These clusters include two cubanes, $Co_4O_4(OAc)_4(py)_4$ (**1A**) and $[Co_4O_4(bpy)_4(OAc)_2]^{2+}$ (**1B**), two "half-cubane" dimers, $[Co_2(OH)_2(OAc)_3(py)_4]^+$ (**2A**) and $[Co_2(OH)_2(OAc)_3(bpy)_2]^+$ (**2B**), and two "incomplete cubane" trimers, $[Co_3O(OH)_2(OAc)_3(py)_5]^{2+}$ (**3A**) and $[Co_3O(OH)_3(OAc)_2(bpy)_3]^{2+}$ (**3B**). Table 1 lists the Co–

Table 1. Selected Atomic Distances from X-ray Diffraction.[23−25]

cluster	O–O distance[a]	range of Co–O distances, Å	range of Co–Co distances, Å
1A	2.56	1.860–1.872	2.696–2.824
1B	n/a	1.863–1.895	2.663–2.850
2A	2.50	1.885–1.893	2.811
2B	2.56	1.883–1.901	2.793
3A	2.49	1.862–1.906	2.780–2.791[b]
3B	2.65	1.880–1.919	2.717–2.874

[a]Estimated, this work (see Supporting Information). [b]We exclude Co–Co not bridged by OH^-.

Co, Co–O, and estimated O–O bond distances for each of these materials based on previous single crystal X-ray diffraction studies.[23−25] All bond lengths are remarkably conserved throughout these clusters, indicating no major structural changes apart from nuclearity per cluster. We report that there is a clear correlation between cluster nuclearity, ligand lability, and catalytic activity among these materials. Specifically, both cubanes **1A** and **1B** are active catalysts for oxygen evolution, differing in specific rates according to the number of labile carboxylate ligands. By contrast, the lower nuclearity clusters are inactive catalysts. Trimer **3A** and dimer **2A** possessing pyridine ligands undergo ligand dissociation that triggers rearrangement to cobalt–oxo oligomers that are active catalysts. These results have significant implications toward understanding the molecular basis by which other reported cobalt complexes may oxidize water.

RESULTS

Catalytic O_2 Evolution from Cubes 1A and 1B. There are several reports of homogeneous water oxidation by **1A**, using the widely adopted photoassay depicted in Scheme 1.[13−15] In light of these reports, **1B** became an interesting candidate to study because the $Co_4O_4^{4+}$ core structure is conserved, but the nature of the coordinating ligands is different. The clusters also differ in charge: **1A** is neutral as isolated, while **1B** is dicationic. To our knowledge, **1B** has not been studied for water oxidation catalysis.

We prepared **1B** as a perchlorate salt according to the literature method.[23] Composition, structure, and purity were established by ^1H NMR, ESI-MS, cyclic voltammetry (CV), and UV–vis (Supporting Information Figures S1–S4). Figure 1 shows the resulting O_2 evolution traces when **1A** and **1B** are used as catalysts with the photoassay of Scheme 1 (pH 8, 0.05 M borate buffer, 1 mM Ru^{2+}, 5 mM persulfate), and dissolved O_2 was monitored by a Clark-type electrode. The amount of O_2 detected exceeded the oxygen content of **1B** at all concentrations measured, indicating that its generation is

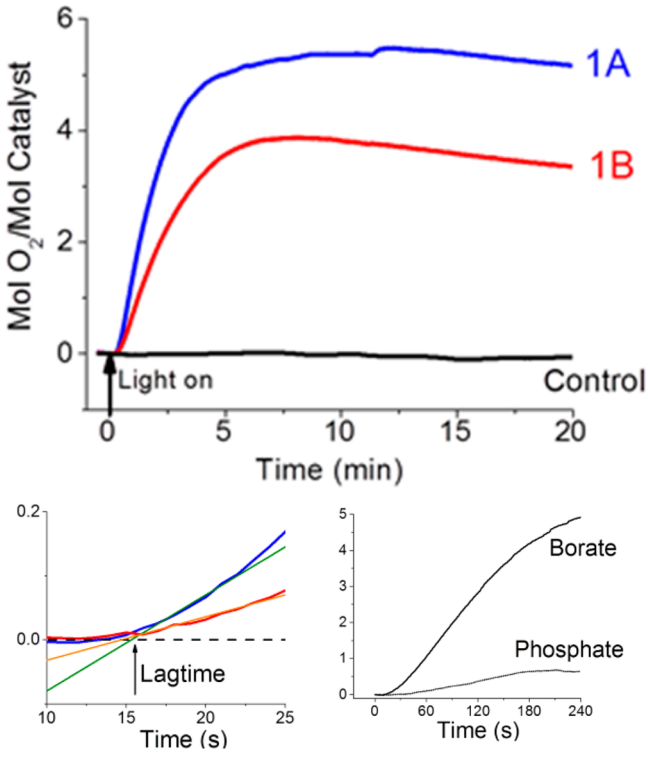

Figure 1. Top: O_2 evolution profiles for **1A** (blue) and **1B** (red) in borate. A control with neither catalyst (black) is also depicted. Lower left: The beginning period of illumination. Intercepts of extrapolated lines for **1A** (green) and **1B** (orange) allow quantification of lag time. Lower right: Profiles of **1A** in pH 8 buffers. Conditions: 100 μM catalyst, 1 mM $Ru(bpy)_3^{2+}$, 5 mM $S_2O_8^{2-}$, 0.05 M buffer, pH 8.

dx.doi.org/10.1021/ic402720p | Inorg. Chem. 2014, 53, 2113−2121

catalytic in nature and not due to stoichiometric decomposition. This conclusion is further supported by the absence of O_2 production in the control lacking either cubane (Figure 1).

When considering cobalt based homogeneous water oxidation catalysts, experiments are required to ensure that the nascent molecular cluster, not decomposition products or cobalt oxide nanoparticles, is the sole source of catalytic O_2 evolution.[26−34] As **1A** has been shown to be stable in the photoassay media under illumination[13] we anticipated that **1B** would be stable as well. To prove this, we compared ^{1}H NMR of **1B** alone (Figure 2 bottom trace), $Ru(bpy)_3^{2+}$ and NaOAc

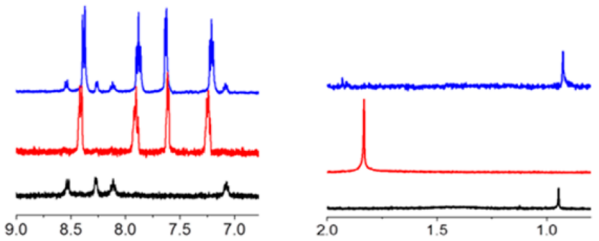

Figure 2. ^{1}H NMR stability of **1B** during catalysis. Black: **1B** alone. Red: $Ru(bpy)_3^{2+}$ and NaOAc. Blue: Contents of photoassay in 90/10 D_2O/H_2O, pH 8 solution (0.01 M in borate) after 10 min of catalysis.

(middle trace), and the contents of the photoassay after 10 min of O_2 evolution from 0.01 M borate buffer in D_2O (top trace). The fact that all peaks present after catalysis can be assigned to either $Ru(bpy)_3^{2+}$ or **1B**, and not free acetate, confirms that **1B** is the source of catalytic O_2 evolution, rather than a decomposed species. ESI-MS also confirms the presence of **1B** in solution after 10 min of catalysis (Supporting Information Figure S5).

When borate buffer is removed from the photoassay conditions in Figure 1, neither **1A** nor **1B** demonstrates catalysis. ^{1}H NMR analysis of this *inactive* solution revealed that *no peaks* of intact cubane (**1A** nor **1B**) are observed after as little as 5 min of illumination. Thus, photodecomposition of cubanes **1A** and **1B** is greatly suppressed in borate. This requirement for a chelating buffer like borate (or carbonate) for cubane catalytic activity may be more than only stability against photodecomposition. Mechanistically, this chelate influence could mean that catalysis may proceed via a base-dependent pathway, involving either deprotonation of an intermediate or hydroxide transfer from borate anion, $B(OH)_4^-$.

Comparative Kinetics: Solvent and Buffer. To test this idea we investigated the dependence of catalytic rate on buffer concentration. Remarkably, addition of borate (pH 8) shows an *inverse* relation between buffer concentration and O_2 evolution rate (Supporting Information Figure S6). While this trend is seemingly counterintuitive, we note that buffer−dye interactions must be present in excess of buffer−catalyst interactions, and that borate is known to accelerate the decomposition of $Ru(bpy)_3^{3+}$ via first-order kinetics (further, the rate constants for this decomposition compare to our observed O_2 evolution constants, suggesting an effect on the same time scale, see below).[35] Further proof of this buffer induced dye decomposition effect is provided in Figure 1, which shows that when borate is replaced at the same pH with phosphate (a faster decomposer of $Ru(bpy)_3^{3+}$),[35] a dramatic decrease in O_2 evolution is observed. Our results agree with a previous report on an observed decrease in quantum yield as borate is replaced with phosphate.[14] Thus, while buffer is required for O_2 evolution and cubane stability against photodecomposition, determination of the reaction order dependence on buffer concentration is complicated by the buffer-dye reaction and the self-terminating nature of the photoassay.

In light of recent reports regarding the sensitive use of conditions when studying homogeneous cobalt water oxidation catalysts, we paid careful attention to the choice of reaction conditions as described next.[30,33,34] For example, the lifetime of the photoassay can be extended to complete consumption of persulfate electron acceptor by using an acetonitrile−water solvent mixture.[15] To directly compare the kinetics of O_2 evolution from **1A** and **1B** we ultimately chose not to pursue this mixed solvent strategy because the potential for one electron oxidation of **1B** in acetonitrile (1.09 V vs SHE) is not equal to that of **1A** (Supporting Information Figure S4); hence, **1A** would receive a thermodynamic advantage. On the other hand, the reduction potentials reported for the $\mathbf{1A}^+/\mathbf{1A}$ and $\mathbf{1B}^+/\mathbf{1B}$ couples in water at pH > 4 are identical (1.25 V vs SHE).[14,36] Thus, while aqueous photoassays do not last to complete persulfate consumption, water-only solvent is used in order to allow for accurate comparison without significant thermodynamic contributions.

Deliberately, we chose not to measure the onset potential for catalytic water oxidation for cubanes **1A** and **1B** via electrochemical methods, as we are currently unable to unambiguously assign the resulting data to solely the intact clusters. In fact, we have observed catalytic CoO_x films formed on the surface of glassy carbon electrodes as a result of decomposition of the cubanes at high potentials on glassy carbon, and we echo other studies[30,34] advising caution if considering studying homogeneous cobalt water oxidation catalysis via electrochemical methods.

While we normally use bicarbonate buffer at pH 7 to screen catalysts (see below), this buffer failed to give consistent kinetic results for **1A** as previously reported.[13] This is due to poorer solubility windows of the photoassay components in concentrated bicarbonate. Despite the change in ligand environment between **1A** and **1B**, the Co_4O_4 core remains a catalytically active structure which acts via a base dependent mechanism. Further comparisons between **1A** and **1B** are presented in the context of the following kinetic analysis.

Lag Time. As can be seen in Figure 1, **1B** evolves O_2 after the lag phase at a slower rate than **1A** over the same time scale. For both materials, the concentration curves plateau at ca. 5 min, after which a steady decrease is observed; this is expected given the self-terminating dye system utilized. To begin a kinetic analysis of these plots, we first consider the lag phase for both materials (Figure 1, inset), during which the assay is illuminated but no O_2 is evolved. The lag time is determined from the intercept of the linear extrapolated fit with the baseline. Under identical conditions, we did not observe noticeable difference between the lag time of **1A** and **1B.** The lag times decrease from 15 to 8 s with increasing $[Ru(bpy)_3^{2+}]$ concentration (Supporting Information Figure S7), consistent with a mechanism that attributes the lag to the time required to photogenerate the oxidant and transfer holes into the cubane catalyst.

Rate Constants. From the slope of the initial linear portion of the plots in Figure 1, the initial rate of O_2 evolution (O_2/s) is obtained. A plot of these rates (μmol/s) versus concentration of catalyst (μmol) gives a straight line for *both* cubanes (Figure 3, top), indicating that the observed catalysis is first-order in

dx.doi.org/10.1021/ic402720p | *Inorg. Chem.* 2014, 53, 2113−2121

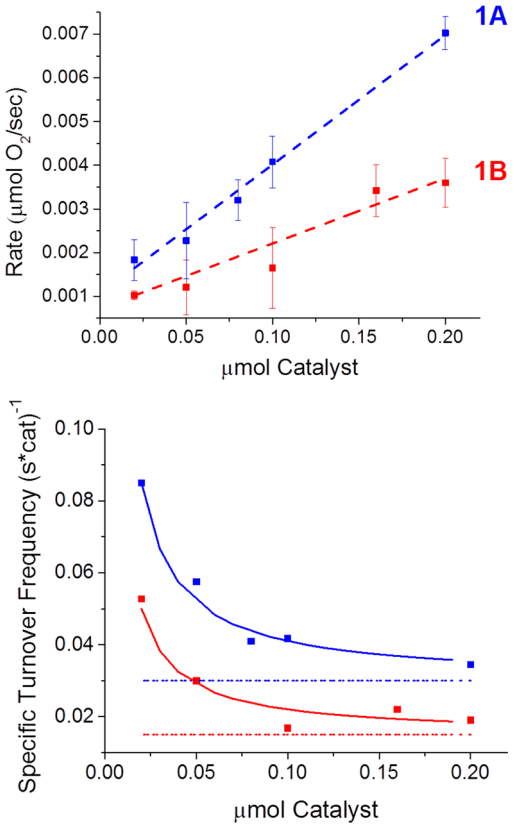

Figure 3. Top: Plot of O_2 evolution rate vs catalyst concentration for **1A** (blue) and **1B** (red). Error bars represent standard deviation of the mean value of each point. Bottom: Plot of TOF vs catalyst concentration for **1A** (blue) and **1B** (red). Dotted lines are the pseudo-first-order rate constants. Solid lines are fits of eqs 2 and 3. At least 6 independent trials are represented per data point.

both **1A** and **1B**. Above catalyst concentrations depicted in Figure 3, the O_2 evolution rate was observed to remain unchanged for each cubane. In this region, the $[Ru(bpy)_3^{2+}]$:[catalyst] ratio is less than 10:1, which we interpret as being nonrepresentative of pseudo-first-order conditions. Hence, because the region in Figure 3 reflects a correlation of rate with concentration of catalyst, the kinetic representation for our data is eq 1:

$$\text{rate} = k[\text{catalyst}]\sum_i [\text{oxidant}]_i + C = k'[\text{catalyst}] + C \quad (1)$$

The slope of the lines in Figure 3 is thus the pseudo-first-order rate constant (k') for each cubane. We obtain values of 0.030 for **1A** and 0.015 mol for **1B** in units of mol O_2 (mol catalyst s)$^{-1}$. However, the y-intercepts are nonzero (C_{1A} = 0.0011, C_{1B} = 0.0007 μmol/s) implying the presence of a zeroth-order pathway. As described next, this zeroth-order contribution is a statistically significant contributor to the overall rate description. First, error analysis of the y-intercepts gives $0.0005 \leq C_{1A} \leq 0.0014$ (95% confidence) and $-0.0002 \leq C_{1B} \leq 0.0012$; these ranges indicate a nonzero y-intercept within experimental error. Second, a log/log plot of the data in Figure 3 gives straight lines with slopes of 0.59 for **1A** and 0.58 for **1B**. This fractional order also indicates the presence of multiple pathways.

Third, we obtain the turnover frequency per catalyst molecule (TOF), by normalizing the rates to the moles of catalyst in solution (Figure 3, bottom). Accurate fits of the data (solid lines) in the resulting plots are constructed only if a significant effect of the nonzero intercept term is included:

$$\text{TOF}_{\mathbf{1A}} = \text{rate}/[\mathbf{1A}] = 0.030 + 0.0011/[\mathbf{1A}] \quad (2)$$

$$\text{TOF}_{\mathbf{1B}} = \text{rate}/[\mathbf{1B}] = 0.015 + 0.0007/[\mathbf{1B}] \quad (3)$$

If the nonzero intercept term is omitted, the fit of solely the pseudo-first-order rate constant (dotted lines, Figure 3, bottom) is poor. We conclude that a zeroth-order pathway exists in this system which is not explained by uncatalyzed O_2 production (Figure 1, control trace). As described next, this pathway is explained by the presence of a multistep mechanism derived from the presence of at least two oxidants from the photoassay medium.

As shown in eqs 2 and 3, an inverse relation between TOF and [catalyst] is seen prominently at low catalyst concentrations. This inverse relationship indicates that catalyst molecules compete with each other for the oxidizing equivalents needed to produce O_2. In light of a previous report which suggested that the sulfate radical contributes to oxidizing **1A**,[14] we suspected this oxidant to be necessary for O_2 evolution.

The sulfate radical is formed *in situ* when excited $Ru(bpy)_3^{2+*}$ is quenched by persulfate (Scheme 1). The $SO_4^{\bullet-}/SO_4^{2-}$ reduction potential is 2.4 V versus SHE,[37] significantly stronger than $Ru(bpy)_3^{3+}/Ru(bpy)_3^{2+}$ (1.26 V vs SHE). As a consequence of the high reduction potential, $SO_4^{\bullet-}$ readily oxidizes $Ru(bpy)_3^{2+}$, **1A**, and the Cl^- counterion.[38] Two experiments verify that $SO_4^{\bullet-}$ is necessary for O_2 evolution. First, addition of excess (>500 equiv) $Ru(bpy)_3(ClO_4)_3$ to solutions of **1A** *failed to produce any* O_2, as monitored by Clark electrode.

Second, a series of photoassays in which 5 mM NaCl or $NaClO_4$ was added prior to illumination was compared to a control with neither salt. As evidenced in Supporting Information Figure S8, addition of $NaClO_4$ gave a reproducible trace indistinguishable from the control with no $NaClO_4$; in contrast, NaCl drastically decreased the rate and yield of O_2 evolution. Chloride oxidation is thermodynamically too high (Cl_2/Cl^-, 1.36 V) to have an impact on any material in the photoassay other than the sulfate radical. Hence, we conclude that, as part of the reaction mechanism, both **1A** and **1B** are oxidized by the sulfate radical in at least one of the four oxidation steps.

The kinetic results further imply a mechanistic feature. Within experimental error, the zeroth-order constants C_{1A} and C_{1B} are both nonzero; however, we cannot distinguish between the two values using their 95% confidence intervals. In contrast, there exists exactly a 2-fold decrease in the observed pseudo-first-order rate constants for **1B** versus **1A**.

This data strongly implies that a rate-limiting step occurs at a Co−OAc binding site, because the number of these coordination sites decreases by 50%. This result agrees with numerous literature reports of labile acetate ligands. Carboxylate exchange on **1B** has been demonstrated synthetically[23] and has been previously utilized to immobilize **1A** on functionalized silica.[39] Insights from EPR studies on both $\mathbf{1A}^{+}$[40] and $\mathbf{1B}^{+}$[41] show that, upon single electron oxidation, the hole is delocalized predominantly across the Co_4O_4 core, residually to the pyridine/bipyridine ligands, and not at all to the acetate, also confirming varying electronic interactions of the ligands on the core. In contrast, our own ^{1}H NMR data

dx.doi.org/10.1021/ic402720p | Inorg. Chem. 2014, 53, 2113−2121

indicate no observable exchange of pyridyl group ligands on the time scale of catalyst turnover. To our knowledge, there are no reports of pyridyl group exchange for either cubane.

Because a base is required for catalysis, we thus conclude that binding of substrate water or hydroxide to a carboxylate site (i.e., an oxo-transfer step) is part of the catalytic mechanism. When coupled to the proof that two species oxidize the cubane, it follows that this oxo-transfer step may occur before or after either oxidation step. These observations thus account for the presence of two observed pathways, one major (in which most catalyst molecules proceed via certain intermediates) and one minor (in which a small amount of catalyst molecules proceed via other intermediates).

One observation which may unify these views is that we cannot eliminate hydroxyl radicals (produced from the quenching reaction of the sulfate radical on water or OH^-) as the additional oxidant.[38] This will be elaborated in discussion.

No Water Oxidation from Incomplete Cubanes. To test whether binuclear "half cubane" and trinuclear "incomplete cubane" analogues of both **1A** and **1B** could act as catalysts for water oxidation, we synthesized and tested two dimers, $[Co_2(OH)_2(OAc)_3(py)_4](PF_6)$ (**2A**) and $[Co_2(OH)_2(OAc)_3(bpy)_2](ClO_4)$ (**2B**), and two trimers, $[Co_3O(OH)_2(OAc)_3(py)_5](PF_6)_2$ (**3A**), and $[Co_3O(OH)_3(OAc)_2(bpy)_3](ClO_4)_2$ (**3B**). Synthesis was conducted by procedures from the literature,[23,25] and all clusters were characterized by ^{1}H NMR and ESI-MS (Supporting Information).

Figure 4 compares representative O_2 evolution profiles for these clusters as measured by Clark electrode (conditions: 0.1 M bicarbonate buffer at pH 7, 0.5 mM $Ru(bpy)_3^{2+}$, 20 mM $S_2O_8^{2-}$ in 90/10 H_2O/MeCN) compared to a blank photoassay (no cobalt). The results are ligand dependent. Both pyridine species (**2A**, **3A**) exhibit O_2 uptake followed by recovery and finally catalytic O_2 evolution after a delay. Both other samples (**2B**, **3B**) and the control are not only catalytically inactive, but also indicate the presence of a reaction that consumes O_2 below the baseline. Given the almost identical structures of **2A** and **2B**, we sought to reconcile this data.

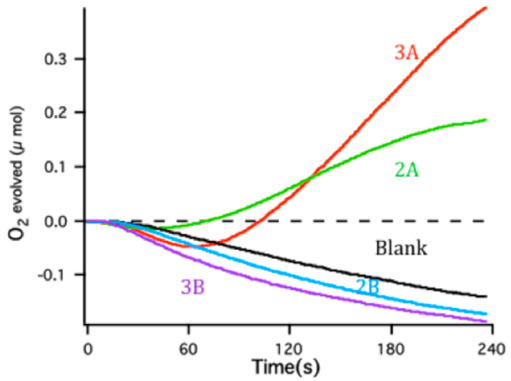

Figure 4. Representative O_2 evolution profiles for lower nuclearity materials as measured by Clark electrode, 0.1 M bicarbonate buffer at pH 7, 0.5 mM $Ru(bpy)_3^{2+}$, 20 mM $S_2O_8^{2-}$ in 90/10 H_2O/MeCN. Cluster concentrations 100 μM. Illumination begins at time t = 0.

Next we present several lines of evidence showing that the pyridyl complexes **2A** and **3A** actually decompose to a different product which does catalyze water oxidation. By contrast, the more stable coordination of bipyridine to both **2B** and **3B** prevents photodecomposition, and neither complex is active catalytically.

Decomposition of 2A and 3A. The observation that complexes **2A** and **3A** take up O_2 from solution under illumination during the long lag phase before catalytic O_2 evolution, in contrast to the profiles of **1A** and **1B**, indicates another reaction(s) occurs. For **2A** and **3A**, the lag times (time to reach the minimum O_2 concentration) were in excess of 30 s and often exceeded 1 min, which compares to the lag times for $Co^{2+} \rightarrow CoO_x$ catalyst under identical conditions.[13] The observed lag times thus suggest that decomposition products, not **2A** and **3A**, are the source of observed O_2 evolution.

Further evidence for decomposition of **2A** and **3A** was obtained by monitoring the photoassay solutions via ^{1}H NMR in 95/5 D_2O/CD_3CN (Figure 5). Before illumination all peaks can be assigned to intact cluster or $Ru(bpy)_3^{2+}$. However, after 10 min of illumination, additional peaks which correlate neither to **2A** nor **3A** are seen in the pyridine and acetate regions. These new peaks do not correspond to free ligands, thus revealing the presence of new molecular species.

Bulk Electrolysis. Electrochemical oxidation allowed definitive attribution of catalytic activity to decomposition product(s) rather than intact **2A** or **3A**, in agreement with the results from photoassay studies. Cyclic voltammetry (CV) of **2A** and **3A** in 0.1 M, pH 7.5 bicarbonate buffer (90/10 H_2O/MeCN) on glassy carbon shows no significant increase in current relative to a blank CV of pure electrolyte. We then electrolyzed solutions of each compound at 1.05 V versus Ag/AgCl, (similar to the redox potential of the $Ru(bpy)_3^{2+/3+}$ couple), and performed cyclic voltammetry of the resulting solutions *with a polished separate electrode*. This ensures that any changes in the electrochemical response of **2A** and **3A** were not simply due to the formation of a heterogeneous cobalt oxide film.

The CV traces of **2A** taken after 0 (red), 3 (blue), 6 (purple), and 12 (green) min of electrolysis show the gradual appearance of a catalytic wave, illustrating the formation of an active homogeneous or suspended species (Figure 6). A similar change was observed for solutions of **3A** (Supporting Information Figure S9). Attempts to isolate and characterize the catalytically active species were unsuccessful. UV−vis of the electrolyzed solutions over time showed disappearance of **2A** and **3A** absorbance features, but failed to identify any new features. ^{1}H NMR of the resulting solution indicated the presence of multiple molecular species (Supporting Information Figure S10), which were not characterized further. These results indicate that **2A** and **3A** are inactive as catalysts and photodecompose or oxidatively rearrange into active species.

Catalytically Inactive Bipyridyl Clusters 2B and 3B. By contrast, tests of O_2 evolution from the bipyridyl species **2B** and **3B** (Figure 4) show low level uptake of O_2 from the photoassay solution even after 10 min of illumination. This O_2 uptake is small (<5%) compared to the yield of catalytic O_2 produced by an equivalent amount of either cubane **1A** or **2A** (Figure 1). We tested this in some detail and found that >50% of the O_2 uptake could be attributed to the photoassay medium, as described in Supporting Information (Figures S11 and S12).

The stark differences between **2A** and **3A**, which decompose to form active materials, versus **2B** and **3B** which show no O_2 evolution, prompted us to investigate the role of the bipyridine ligand in suppressing catalytic O_2 evolution. Bpy has been previously noted to poison amorphous CoO_x which may form *in situ*, and can serve as a ligand to determine the origin of

dx.doi.org/10.1021/ic402720p | Inorg. Chem. 2014, 53, 2113−2121

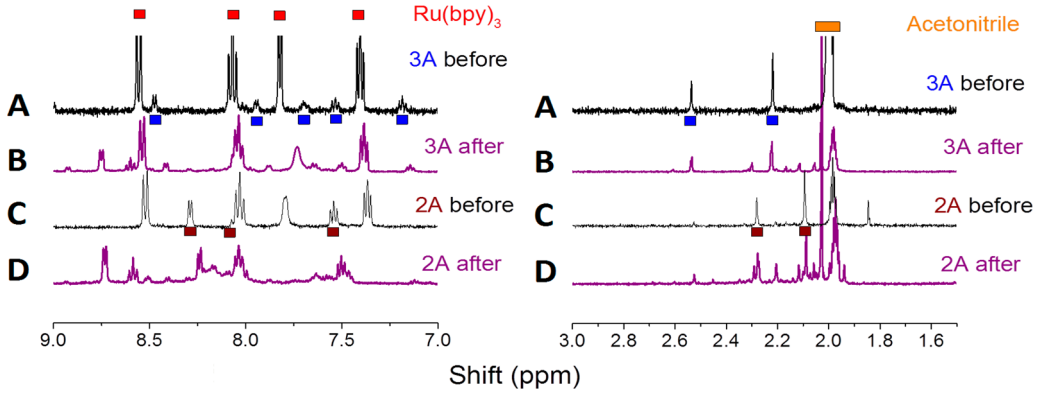

Figure 5. ^{1}H NMR stability tests of **2A** and **3A** before and after 10 min of illumination in 95/5 D_2O/CD_3CN, 0.05 M pH 8 borate buffer. Lines A and C are before measurements, lines B and D are after.

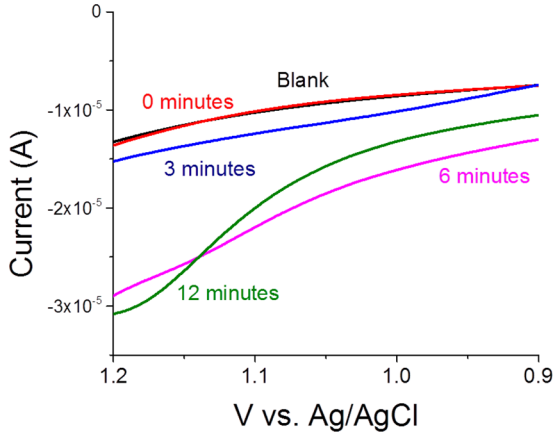

Figure 6. Linear voltammetry of 0.2 mM of **2A** in 0.1 M pH 7.5 bicarbonate (90/10 H_2O/CH_3CN) after various electrolysis times (1.05 V vs Ag/AgCl). The black trace corresponds to blank electrolyte.

catalytic activity.[9] Titration of bipyridine into the photoassay medium containing the pyridyl complex **2A** (Figure 7)

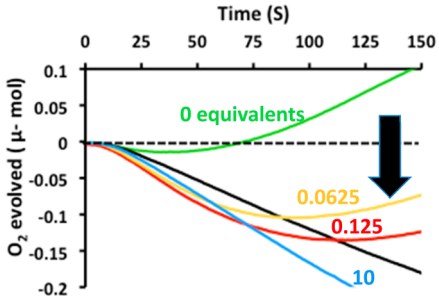

Figure 7. Clark electrode traces of 0.1 mM solutions of **2A** with equivalents of bipyridine. The black trace is a control (no **2A**) as reference. Conditions: 0.1 M bicarbonate buffer (pH 7), 0.5 mM $Ru(bpy)_3^{2+}$, 20 mM $S_2O_8^{2-}$, 90/10 H_2O/CH_3CN.

significantly increases the lag time preceding net O_2 evolution from 30 s (0 equiv bpy), to 90 s (0.0625 equiv, yellow), to 110 s (0.125 equiv, red). When excess bpy (>5 equiv) is added no net O_2 evolution is observed up to 5 min of illumination, and the O_2 profiles largely resemble those of **2B** and **3B** (Supporting Information Figure S13). On the other hand, titration of free bpy into **2B** or **3B** showed no further changes (Supporting Information Figure S14), indicating that free bpy alone is not responsible for O_2 uptake. Thus, we propose that the weak O_2 consumption exhibited by **2B**/**3B**, and **2A**/**3A** in the presence of bpy, is consistent with irreversible oxidation of bpy chelated to cobalt, possibly by attack of an oxo/hydroxo ligand on the bpy. Further, bpy chelation to these precursor complexes slows or prevents them from forming the active CoO_x decomposition product.

DISCUSSION

We have shown that, in neutral and near neutral pH conditions, two fully assembled cubane motifs, **1A** and **1B**, are intrinsically active catalysts for water oxidation, and that their relative rates scale precisely with the number of labile carboxylate sites. By contrast, molecular cobalt−oxo clusters of lower nuclearity (half cubane dimers and incomplete cubane trimers) are catalytically inactive, even though both dimers and trimers have bridging oxos and labile carboxylate sites where terminal water molecules may exchange. Comparing the activity of the compounds tested in this study to the structural parameters listed in Table 1 reveals that the O−O, Co−O, and Co−Co bond distances are largely conserved across all clusters tested. Thus, no major changes in bond distances are responsible for the sudden appearance of O_2 production as Co nuclearity increases to four in both these series. We conclude that a four-electron oxidation pathway is not accessible in these dimers and trimers, and that the Co_4O_4 cubane topology provides the necessary pathway for activation and O−O bond formation.

Our report of inactivity from organo-cobalt clusters with nuclearity less than 4 stands in contrast to reports of catalytic activity from several organo-Co_2O_2 dimers[42] and Co monomers.[28,43−48] The proposed mechanisms for these materials from their original literature are presented in Scheme 2. To our knowledge, a nucleophilic attack mechanism of water or hydroxide is proposed for all the catalytic monomers.[28,43−47] Since these studies are performed at pH ≥ 7, we depict hydroxide as the attacking substrate (Scheme 2, top) for simplicity. The oxidation state of the catalyst that is immediate precursor to O−O bond formation is uncertain, and different claims have been made. For example, Berlinguette et al. and Sartorel et al. postulate Co^{4+}—OH and Co^{4+}=O, respectively, in their systems;[28,43,45] these are both formally $1e^-$ above a Co^{3+}—OH moiety. On the other hand, Nocera et al. and Groves et al. propose $2e^-$ above Co^{3+}—OH in their systems; their catalysts are abbreviated $^{\bullet}$L—Co^{4+}—OH, where the second hole is ligand-centered.[46,47] The reasons for these

dx.doi.org/10.1021/ic402720p | Inorg. Chem. 2014, 53, 2113−2121

Scheme 2. Proposed Mechanisms of Water Oxidation by Other Cobalt Clusters[28,42−47] and Theoretical Calculations (Bottom)[48]

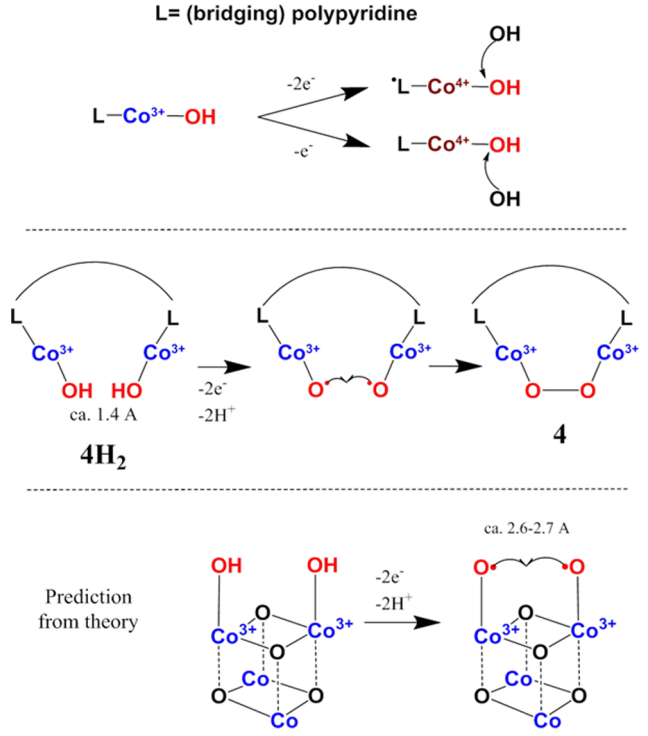

differences are not known, but may reflect their different coordination environments.

It becomes apparent upon increasing cobalt nuclearity that multiple metals may contribute to the O−O bond formation step, as opposed to tailoring the electronic environment around a single, active metal center. This is evidenced in the proposed mechanism for the known dimer catalysts (Scheme 2, middle). $[Co(L)]_2(\mu\text{-bpp})(\mu\text{-}1,2\text{-}O_2)^{3+}$ (L= terpyridine or bis-*N*(methyl-imidazoyl)pyridine, bpp = bispyridylpyrazolate) each contains a bound peroxo, $Co^{3+}—O—O—Co^{3+}$, when isolated.[42] We label this structure **4** in Scheme 2. During catalytic turnover, the proposed reduced intermediate $\mathbf{4H_2}$ consists of two terminal Co^{3+}—OH groups. The first two oxidations generate two $Co^{3+}—O^{\bullet}$ in which the unpaired electron occupies an antibonding $2p\pi$ orbital on oxygen. (This electronic configuration is formally equivalent to Co^{4+}═O, in which an electron is promoted from a filled $3d\pi$ orbital on Co to fill the π bonding orbital to oxygen that is denoted by the double bond. An unpaired electron exists in the $(3d)t_{2g}^5$ orbitals on Co, formally denoted Co^{4+}. For simplicity, we retain the oxo radical notation here.) Unlike the nucleophilic attack mechanism, the peroxo bond is formed via coupling of the two $Co^{3+}—O^{\bullet}$ groups. This mechanism has been postulated to occur for the Co_4O_4 cubane with an energy barrier of 2.3 kcal/mol based on DFT calculations[48] (Scheme 2, bottom). We note that this cross-coupling mechanism indirectly implies that a single $Co^{3+}—O^{\bullet}$ (equivocally Co^{4+}═O) is insufficient to oxidize water via a nucleophilic attack mechanism. This is substantiated by several Co^{3+}−OOR alkylperoxide systems, in which the $Co^{3+}—O^{\bullet}$ generated by homolytic bond cleavage is a weaker oxidant of hydrocarbons than the counterpart $^{\bullet}$OR.[49−51]

Applying these parameters to our system, we note that all intramolecular O−O bond distances are conservatively estimated to be ca. 2.5 Å, a full angstrom longer than peroxo bonds (Table 1). For this reason, intramolecular coupling between *bridging* O−O is unfavorable in *any* of our compounds (active and inactive). An alternate possibility for intramolecular *terminal* O−O coupling can be envisioned (as in Scheme 2, bottom). However, this requires *full* dissociation of a (bidentate) acetate, and must occur over Co−Co distances in the range ca. 2.6−2.8 Å (Table 1). A recent study reports only a small contraction (0.03 Å) of some Co−Co distances from **1A** to $\mathbf{1A}^+$, indicating this Co−Co distance remains relatively long upon hole injection.[52] Combined with the lack of free acetate detection in solution, these lines of evidence suggest that the catalytic mechanism for **1A** and **1B** is not cross-coupling of two $Co^{3+}—O^{\bullet}$ moieties. From this we conclude that intramolecular O−O bond distance is the primary structural feature needed for water oxidation by cobalt *dimers*.

We propose that efficient hole delocalization, which facilitates buildup of oxidizing equivalents on cobalt, is the defining property of catalysis from the Co_4O_4 cubane. This is emphasized for **1A** in acetonitrile, where an electron can be removed electrochemically from the core at ca. 0.7 V versus Ag/AgCl, reversibly forming Co_4(3III,IV). In contrast, electrochemical hole injection into either **2A** or **3A** is not seen up to 1.5 V versus Ag/AgCl (Supporting Information Figure S15). This effect we believe is more intrinsic to the core type as opposed to the varying cluster charge (**1A** is neutral, **2A** and **3A** are cations) because the 2+ cation **1B** is also reversibly oxidized within this window (Supporting Information Figure S4).

Our proposed mechanism presented in Scheme 3 accounts for our experimental observations and highlights the effective

Scheme 3. Proposed Mechanism for Water Oxidation by the Co_4O_4 Cubane (This Work)

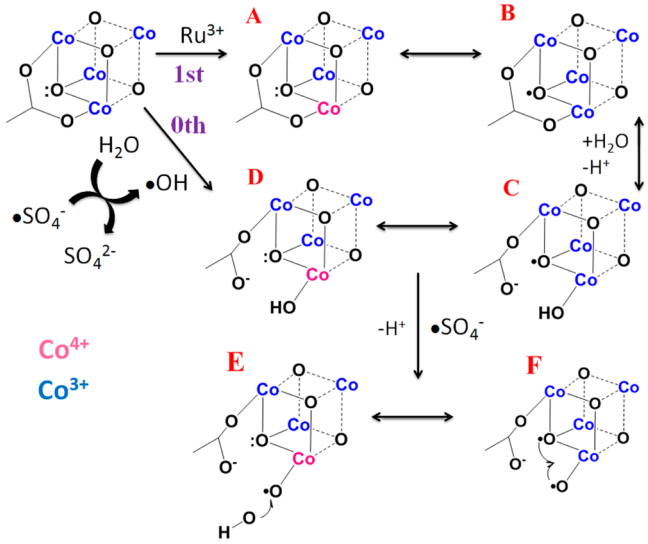

hole delocalization properties of the cubane structure. The first-order pathway is assigned to oxidation of cubane **1** by Ru^{3+}; this occurs quickly (10^7 $(M\ s)^{-1}$),[14] and hence $[1]_o \approx [1^+]$. Due to the known properties of $\mathbf{1}^+$ with both ligand sets, the hole is delocalized across the core, though we depict this in the form of resonance where the hole lies on a cobalt (A) or an oxo bridge (B). Generation of a terminal hydroxide at a carboxylate site then occurs (C), which gives an intermediate that is also

dx.doi.org/10.1021/ic402720p | Inorg. Chem. 2014, 53, 2113−2121

accessible via attack by (persulfate generated) $^{\bullet}$OH in the proposed zeroth-order pathway (D).

Experimental and computational results suggest that a range of potentials for oxidation of a catalyst containing Co^{4+}−OH is 1.4−1.5 V versus SHE,[43,46,48] which is too high for $Ru(bpy)_3^{3+}$ (1.26 V), but not $SO_4^{\bullet-}$ (2.4 V). Thus, the sulfate radical is the only oxidant of sufficient strength to perform the next PCET step on the terminal hydroxide, and a base is required to remove the proton. Depending on resonance, this gives (formally) a terminal Co^{4+}−$O^{\bullet}$ (E), or one bridging and one terminal $O^{\bullet}$ connected by a Co^{3+} center (F). The O−O bond formation step thus proceeds via nucleophilic attack of hydroxide in the former case, or oxo−oxyl radical coupling in the latter case. We do not yet have single turnover ^{18}O data that might distinguish these pathways, but we note that the need for a base in our system suggests either one or two oxo substrates originate from bulk water. For either peroxo product, subsequent two electron oxidation would generate the O_2 product and regenerate the starting Co_4O_4 cubane.

The oxo−oxyl radical coupling mechanism (F) in particular has been proposed by our group to occur in Photosystem II,[53] and is favored in recent EPR studies.[54] This mechanism may account for the isotope labeling studies which found oxos from the Co-Pi catalyst incorporated into product O_2.[55] Depending on the resonance stabilization observed in the cubane, either or both mechanisms may occur simultaneously.

As a final note, **1A** and **1B** compare to the structurally similar $Co^{II}_4(hmp)_4(\mu\text{-}OAc)_2(H_2O)_2$ (hmp = 2-hydroxymethyl pyridine) cubane catalyst, but have lower TOFs under similar conditions.[56] A similar derivative to **1A** has been demonstrated to last for 3 times as many turnovers.[15] We ascribe the slower rates of catalysis from **1A** and **1B** as due to the need to displace an acetate ligand in order to generate a terminal oxo, as precursor to O_2 evolution. However, the ligand environment of **1A** allows for greater catalyst longevity as the terminal aquo form is unstable toward decomposition which results in lower turnover numbers.

CONCLUSION

The molecular clusters studied herein represent discrete models of various cobalt oxide water oxidation catalysts including the solid state spinels. In particular, we have compared the Co_4O_4 cubane structure with smaller subclusters, including Co_2O_2 and $Co_3O_{3,4}$ cores, and conclude on the basis of multiple lines of evidence that none of these smaller subclusters is catalytically active for O_2 evolution from water. The origin of catalytic activity by Co_4O_4 cubanes illustrates three key features for water oxidation: (1) four one-electron redox metals, (2) efficient charge delocalization of the first oxidation step across the Co_4O_4 cluster, allowing for stabilization of higher oxidizing equivalents, and (3) terminal coordination site for substrate aquo/oxo formation.

Our findings also illustrate the complexity of the $Ru(bpy)_3^{2+}$/$S_2O_8^{2-}$ photoassay, since we have shown that persulfate and buffer are both necessary for catalysis outside of their "standard" roles as sacrificial electron and proton acceptors, respectively.

ASSOCIATED CONTENT

Supporting Information

Detailed synthetic procedures, characterization, illumination profile, and estimation of O−O bond distances. This material is available free of charge via the Internet at http://pubs.acs.org.

AUTHOR INFORMATION

Corresponding Author

*E-mail: dismukes@rci.rutgers.edu.

Author Contributions

†These authors contributed equally to this report.

Notes

The authors declare no competing financial interest.

ACKNOWLEDGMENTS

We thank Clyde Cady, Anders Laursen, David Vinyard, and Jennifer Sun for discussions, and Nagarajan Murali and Gennady Ananyev for instrument support. This work was supported by the Air Force Office of Scientific Research (Grant FA9550-11-1-0231). P.F.S. acknowledges partial support from an NSF IGERT fellowship. C.K. acknowledges partial fellowship support from the Rutgers University Aresty Research Center and Rutgers Energy Institute. D.M.R. and N.M. acknowledge partial fellowship support from Rutgers University.

REFERENCES

(1) Kent, C. A.; Concepcion, J. J.; Dares, C. J.; Torelli, D. A.; Rieth, A. J.; Miller, A. S.; Hoertz, P. G.; Meyer, T. J. *J. Am. Chem. Soc.* **2013**, *135*, 8432−8435.

(2) Young, K. J.; Martini, L. A.; Milot, R. L.; Snoeberger, R. C., III; Batista, V. S.; Schmuttenmaer, C. A.; Crabtree, R. H.; Brudvig, G. W. *Coord. Chem. Rev.* **2012**, *256*, 2503−2520.

(3) Lin, X.; Hu, X.; Concepcion, J. J.; Chen, Z.; Liu, S.; Meyer, T. J.; Yang, W. *Proc. Natl. Acad. Sci. U.S.A.* **2012**, *109*, 15669−15672.

(4) Gao, Y.; Crabtree, R. H.; Brudvig, G. W. *Inorg. Chem.* **2012**, *51*, 4043−4050.

(5) Ellis, W. C.; McDaniel, N. D.; Bernhard, S.; Collins, T. J. *J. Am. Chem. Soc.* **2010**, *132*, 10990−10991.

(6) Barnett, S. M.; Goldberg, K. I.; Mayer, J. M. *Nat. Chem.* **2012**, *4*, 498−502.

(7) Chen, Z.; Meyer, T. J. *Angew. Chem., Int. Ed.* **2013**, *52*, 700−703.

(8) Joya, K. S.; Vallés-Pardo, J. L.; Joya, Y. F.; Eisenmayer, T.; Thomas, B.; Buda, F.; de Groot, H. J. M. *ChemPlusChem* **2013**, *78*, 35−47.

(9) Yin, Q.; Tan, J. M.; Besson, C.; Geletii, Y. V; Musaev, D. G.; Kuznetsov, A. E.; Luo, Z.; Hardcastle, K. I.; Hill, C. L. *Science* **2010**, *328*, 342−345.

(10) Duan, L.; Bozoglian, F.; Mandal, S.; Stewart, B.; Privalov, T.; Llobet, A.; Sun, L. *Nat. Chem.* **2012**, 1−6.

(11) Umena, Y.; Kawakami, K.; Shen, J.-R.; Kamiya, N. *Nature* **2011**, *473*, 55−60.

(12) Sartorel, A.; Bonchio, M.; Campagna, S.; Scandola, F. *Chem. Soc. Rev.* **2013**, *42*, 2262−2280.

(13) McCool, N. S.; Robinson, D. M.; Sheats, J. E.; Dismukes, G. C. *J. Am. Chem. Soc.* **2011**, *133*, 11446−11449.

(14) La Ganga, G.; Puntoriero, F.; Campagna, S.; Bazzan, I.; Bonchio, M.; Sartorel, A.; Natali, M.; Scandola, F. *Faraday Discuss.* **2012**, *155*, 177−190.

(15) Berardi, S.; Natali, M.; Bazzan, I.; Puntoriero, F.; Sartorel, A.; Scandola, F.; Campagna, S.; Bonchio, M. *J. Am. Chem. Soc.* **2012**, *134*, 11104−11107.

(16) Swiegers, G. F.; Clegg, J. K.; Stranger, R. *Chem. Sci.* **2011**, *2*, 2254−2262.

(17) Jiao, F.; Frei, H. *Angew. Chem., Int. Ed.* **2009**, *48*, 1841−1844.

(18) Robinson, D. M.; Go, Y. B.; Greenblatt, M.; Dismukes, G. C. *J. Am. Chem. Soc.* **2010**, *132*, 11467−11469.

(19) Gardner, G. P.; Go, Y. B.; Robinson, D. M.; Smith, P. F.; Hadermann, J.; Abakumov, A.; Greenblatt, M.; Dismukes, G. C. *Angew. Chem.* **2012**, *124*, 1648−1651.

(20) Kanan, M. W.; Yano, J.; Surendranath, Y.; Dinca, M.; Yachandra, V. K.; Nocera, D. G. *J. Am. Chem. Soc.* **2010**, *132*, 13692−13701.

(21) Risch, M.; Khare, V.; Zaharieva, I.; Gerencser, L.; Chernev, P.; Dau, H. *J. Am. Chem. Soc.* **2009**, *131*, 6936−6937.
(22) Du, P.; Kokhan, O.; Chapman, K. W.; Chupas, P. J.; Tiede, D. M. *J. Am. Chem. Soc.* **2012**, *134*, 11096−11099.
(23) Dimitrou, K.; Folting, K.; Streib, W. E.; Christou, G. *J. Am. Chem. Soc.* **1993**, *115*, 6432−6433.
(24) Chakrabarty, R.; Bora, S. J.; Das, B. K. *Inorg. Chem.* **2007**, *46*, 9450−9462.
(25) Sumner, C. E. *Inorg. Chem.* **1988**, *27*, 1320−1327.
(26) Shevchenko, D.; Anderlund, M. F.; Thapper, A.; Styring, S. *Energy Environ. Sci.* **2011**, *4*, 1284−1287.
(27) Tanaka, S.; Annaka, M.; Sakai, K. *Chem. Commun.* **2012**, *48*, 1653−1655.
(28) Wasylenko, D. J.; Palmer, R. D.; Schott, E.; Berlinguette, C. P. *Chem. Commun.* **2012**, *48*, 2107−2109.
(29) Natali, M.; Berardi, S.; Sartorel, A.; Bonchio, M.; Campagna, S.; Scandola, F. *Chem. Commun.* **2012**, *48*, 8808−8810.
(30) Stracke, J. J.; Finke, R. G. *J. Am. Chem. Soc.* **2011**, *133*, 14872−14875.
(31) Brunschwig, B. S.; Chou, M. H.; Creutz, C.; Ghosh, P.; Sutin, N. *J. Am. Chem. Soc.* **1983**, *105*, 4832−4833.
(32) Artero, V.; Fontecave, M. *Chem. Soc. Rev.* **2013**, *42*, 2338−2356.
(33) Vickers, J. W.; Lv, H.; Sumliner, J. M.; Zhu, G.; Luo, Z.; Musaev, D. G.; Geletii, Y. V; Hill, C. L. *J. Am. Chem. Soc.* **2013**, *135*, 14110−14118.
(34) Stracke, J. J.; Finke, R. G. *ACS Catal.* **2013**, *3*, 1209−1219.
(35) Hara, M.; Waraksa, C. C.; Lean, J. T.; Lewis, B. A.; Mallouk, T. E. *J. Phys. Chem. A* **2000**, *104*, 5275−5280.
(36) Symes, M. D.; Surendranath, Y.; Lutterman, D. A.; Nocera, D. G. *J. Am. Chem. Soc.* **2011**, *133*, 5174−5177.
(37) Parent, A. R.; Crabtree, R. H.; Brudvig, G. W. *Chem. Soc. Rev.* **2013**, *42*, 2247−2252.
(38) Waldemer, R. H.; Tratnyek, P. G.; Johnson, R. L.; Nurmi, J. T. *Environ. Sci. Technol.* **2006**, *41*, 1010−1015.
(39) Sarmah, P.; Chakrabarty, R.; Phukan, P.; Das, B. K. *J. Mol. Catal. A: Chem.* **2007**, *268*, 36−44.
(40) McAlpin, J. G.; Stich, T. A.; Ohlin, C. A.; Surendranath, Y.; Nocera, D. G.; Casey, W. H.; Britt, R. D. *J. Am. Chem. Soc.* **2011**, *133*, 15444−15452.
(41) Dimitrou, K.; Brown, A. D.; Concolino, T. E.; Rheingold, A. L.; Christou, G. *Chem. Commun.* **2001**, 1284−1285.
(42) Rigsby, M. L.; Mandal, S.; Nam, W.; Spencer, L. C.; Llobet, A.; Stahl, S. S. *Chem. Sci.* **2012**, *3*, 3058−3062.
(43) Wasylenko, D. J.; Ganesamoorthy, C.; Borau-Garcia, J.; Berlinguette, C. P. *Chem. Commun.* **2011**, *47*, 4249−4251.
(44) Leung, C.-F.; Ng, S.-M.; Ko, C.-C.; Man, W.-L.; Wu, J.; Chen, L.; Lau, T.-C. *Energy Environ. Sci.* **2012**, *5*, 7903−7907.
(45) Pizzolato, E.; Natali, M.; Posocco, B.; Montellano Lopez, A.; Bazzan, I.; Di Valentin, M.; Galloni, P.; Conte, V.; Bonchio, M.; Scandola, F.; Sartorel, A. *Chem. Commun.* **2013**, *49*, 9941−9943.
(46) Wang, D.; Groves, J. T. *Proc. Natl. Acad. Sci. U.S.A.* **2013**, *110*, 15579−15584.
(47) Dogutan, D. K.; McGuire, R.; Nocera, D. G. *J. Am. Chem. Soc.* **2011**, *133*, 9178−9180.
(48) Wang, L.-P.; Van Voorhis, T. *J. Phys. Chem. Lett.* **2011**, *2*, 2200−2204.
(49) Chavez, F. A.; Rowland, J. M.; Olmstead, M. M.; Mascharak, P. K. *J. Am. Chem. Soc.* **1998**, *120*, 9015−9027.
(50) Chavez, F. A.; Mascharak, P. K. *Acc. Chem. Res.* **2000**, *33*, 539−545.
(51) Zhang, J.; Biradar, A. V; Pramanik, S.; Emge, T. J.; Asefa, T.; Li, J. *Chem. Commun.* **2012**, *48*, 6541−6543.
(52) Stich, T.; Krzystek, J.; Mercardo, B. Q.; McAlpin, J. G.; Ohlin, C. A.; Olmstead, M. M.; Casey, W. H.; Britt, R. D. *Polyhedron* **2013**, *64*, 304−307.
(53) Vinyard, D. J.; Ananyev, G. M.; Dismukes, G. C. *Annu. Rev. Biochem.* **2013**, *82*, 577−606.
(54) Pérez Navarro, M.; Ames, W. M.; Nilsson, H.; Lohmiller, T.; Pantazis, D. A.; Rapatskiy, L.; Nowaczyk, M. M.; Neese, F.; Boussac, A.; Messinger, J.; Lubitz, W.; Cox, N. *Proc. Natl. Acad. Sci. U.S.A.* **2013**, *110*, 15561−15566.
(55) Surendranath, Y.; Kanan, M. W.; Nocera, D. G. *J. Am. Chem. Soc.* **2010**, *132*, 16501−16509.
(56) Evangelisti, F.; Güttinger, R.; Moré, R.; Luber, S.; Patzke, G. R. *J. Am. Chem. Soc.* **2013**, *135*, 18734−18737.